

Model Inversion Attack via Dynamic Memory Learning

Gege Qi
qigege.qgg@alibaba-inc.com
Alibaba Group
Hang Zhou, China

YueFeng Chen
yuefeng@alibaba-inc.com
Alibaba Group
Hang Zhou, China

Xiaofeng Mao
mxf164419@alibaba-inc.com
Alibaba Group
Hang Zhou, China

Binyuan Hui
binyuan.hby@alibaba-inc.com
Alibaba Group
Beijing, China

Xiaodan Li
fiona.lxd@alibaba-inc.com
Alibaba Group
Hang Zhou, China

Rong Zhang
stone.zhangr@alibaba-inc.com
Alibaba Group
Hang Zhou, China

Hui Xue
hui.xueh@alibaba-inc.com
Alibaba Group
Hang Zhou, China

ABSTRACT

Model Inversion (MI) attacks aim to recover the private training data from the target model, which has raised security concerns about the deployment of DNNs in practice. Recent advances in generative adversarial models have rendered them particularly effective in MI attacks, primarily due to their ability to generate high-fidelity and perceptually realistic images that closely resemble the target data. In this work, we propose a novel Dynamic Memory Model Inversion Attack (DMMIA) to leverage historically learned knowledge, which interacts with samples (during the training) to induce diverse generations. DMMIA constructs two types of prototypes to inject the information about historically learned knowledge: Intra-class Multicentric Representation (IMR) representing target-related concepts by multiple learnable prototypes, and Inter-class Discriminative Representation (IDR) characterizing the memorized samples as learned prototypes to capture more privacy-related information. As a result, our DMMIA has a more informative representation, which brings more diverse and discriminative generated results. Experiments on multiple benchmarks show that DMMIA performs better than state-of-the-art MI attack methods.

CCS CONCEPTS

• **Computing methodologies** → **Computer vision problem.**

KEYWORDS

Model Inversion Attack, Intra-class Multicentric Representation, Inter-class Discriminative Representation

This research is supported in part by the National Key Research and Development Program of China under Grant No.2020AAA0140000.

Permission to make digital or hard copies of all or part of this work for personal or classroom use is granted without fee provided that copies are not made or distributed for profit or commercial advantage and that copies bear this notice and the full citation on the first page. Copyrights for components of this work owned by others than the author(s) must be honored. Abstracting with credit is permitted. To copy otherwise, or republish, to post on servers or to redistribute to lists, requires prior specific permission and/or a fee. Request permissions from [permissions@acm.org](https://www.acm.org/permissions).

MM '23, October 29–November 3, 2023, Ottawa, ON, Canada

© 2023 Copyright held by the owner/author(s). Publication rights licensed to ACM.
ACM ISBN 979-8-4007-0108-5/23/10...\$15.00
<https://doi.org/10.1145/3581783.3612072>

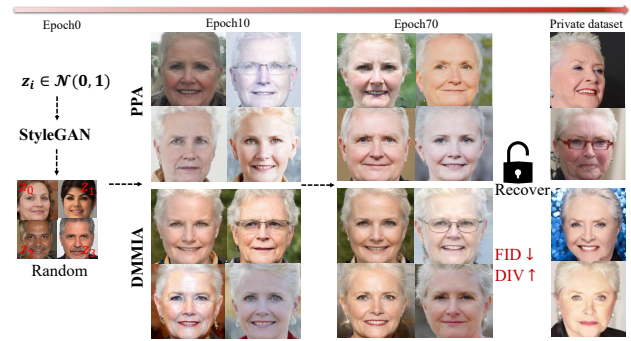


Figure 1: Comparison between DMMIA and the baseline model inversion attack. DMMIA has higher sample diversity while achieving more accurate privacy data reconstructions. In this example, our method can preserve more characteristics (e.g., glasses) of the target class during optimization.

ACM Reference Format:

Gege Qi, YueFeng Chen, Xiaofeng Mao, Binyuan Hui, Xiaodan Li, Rong Zhang, and Hui Xue. 2023. Model Inversion Attack via Dynamic Memory Learning. In *Proceedings of the 31st ACM International Conference on Multimedia (MM '23)*, October 29–November 3, 2023, Ottawa, ON, Canada. ACM, New York, NY, USA, 9 pages. <https://doi.org/10.1145/3581783.3612072>

1 INTRODUCTION

Deep neural networks (DNNs) have achieved great success in a wide range of applications, including facial recognition [28, 30], personalized medicine [31] and product recommendation [38]. However, the fact that privacy-sensitive applications of DNNs increasingly utilize sensitive and proprietary information raised great concerns about privacy. Recently, [9] proposed a model inversion (MI) attack aiming to reconstruct sensitive features of private training data by leveraging their correlation with the model output. The study highlights the vulnerability of linear regression models used in personalized medicine to such attacks, leading to the disclosure of confidential genomic data of individual patients.

While MI attacks have traditionally been limited to discrete signals, recent advances have extended the attack to high-dimensional

and continuous signals such as image data using Generative Adversarial Networks (GANs) [4, 14, 44]. However, the effectiveness of GAN-based MI attacks is limited by an infamous problem called "catastrophic forgetting" [24]. In MI attacks, as shown in Figure 1, this tendency is expressed as that the generated samples from early updating epochs contain more characteristics (e.g., glasses), but some are dropped during training progress. This property leads to poor attack performance and limited diversity in generation results.

One common approach to mitigate catastrophic forgetting in GANs is to employ a progressive training strategy, which involves gradually adding new characteristics to the generated samples while preserving previously learned ones, such as gradient penalties [36]. Another approach is to use a memory module that can store and recall previously learned information [5]. Our approach leverages memory replay mechanisms to maintain previously learned features while adapting to new characteristics, resulting in more effective MI attacks and increased diversity in generated samples. By addressing the issue of forgetting in GAN-based MI attacks, our work represents a significant step forward in the development of efficient MI attacks without modifying the architecture of GANs.

Towards this end, we propose a novel MI attack leveraging a Dynamic Memory Mechanism, which effectively reuses the memory of the inversion data by prototype learning, named as DMMIA. Specifically, a prototype is defined as "a representative embedding for a group of semantically similar instances." DMMIA composes two types of prototypes, which are designed to memorize intra- and inter-classes information, respectively. In detail: (1) **Intra-class Multicentric Representation (IMR)**: IMR uses multiple centers stored by prototypes to present the concept of the target class, which increases the sample diversity from the perspective of intra-class relationships. (2) **Inter-class Discriminative Representation (IDR)**: Given a specific class, it stores the historical knowledge of previously synthesized images and enforces the embedding feature of a sample to be more similar to its corresponding prototypes compared to other prototypes.

Along with progressively-updated prototypes, DMMIA can well preserve the diversity of the target compared with the previous method, as shown in Figure 1. However, one might wonder why this memory mechanism is helpful in increasing sample diversity. We perform a theoretical study on the sample diversity of DMMIA. In fact, the floor level of the geodesic distance (the shortest path between the vertices) between any two generated images is larger than that without proposed prototypes (see Section 5). It confirms that DMMIA can preserve more diversities of the target distribution.

We perform extensive experiments with both sensitive face and natural datasets, diverse model architectures, and different levels of image prior. Experimental results validate that DMMIA improves the attack success rate and can synthesize high fidelity and diverse images. Towards attacks with and without high-quality image prior, we outperform state-of-the-art methods by up to 6.26% and 20.8% accuracy rates respectively. Our contributions are as follows:

- We propose a novel dynamic memory model inversion attack (DMMIA), which applies an Intra-class Multicentric Representation (IMR) term and an Inter-class Discriminative Representation (IDM) term to model the representation of target classes by memory induction.

- We give both theoretical and empirical insights to validate DMMIA's effectiveness.
- Our proposed DMMIA achieves new state-of-the-art attack performance on multiple benchmarks.

2 RELATED WORK

Catastrophic forgetting. Methods for overcoming catastrophic forgetting can be categorized as: (1) Continual learning-based methods, like EWC [21], aim to minimize weight changes in critical areas for previous tasks by estimating the diagonal empirical Fisher information matrix. Based on EWC, [32] has explored label-conditioned image generation to enhance image realism. However, it faces challenges in generating high-quality images. Lifelong GAN [42] utilizes knowledge distillation to transfer knowledge from prior networks to the news. Piggyback GAN [41] is a parameter-efficient approach by weight reusing when extending a trained network to new tasks. These methods aim to enable models to adapt to new tasks without knowledge forgetting. However, MI attacks focus on exploiting vulnerabilities in the model's behavior to extract sensitive information rather than preserving knowledge across tasks. (2) Incremental learning is a relatively work to study the problem of catastrophic forgetting. DCIGAN [11] uses a GAN generator to store the information of past data and continuously update GAN parameters with new data. For MI attacks, learning about the target data is an incremental process, making it challenging to train auxiliary GANs to record historical information effectively. (3) Our work aligns with the concept of memory replay, where images from a model trained on previous tasks are combined with current training images for updates.

Model inversion attacks. Our work aims to recover private training data or sensitive attributes from access to a trained model. One of the earliest MI attacks specific to a linear regression model was proposed on genomic privacy [10]. For threat models with high-dimensional inputs, [9] first used gradient descent to solve the underlying attack optimization problem. To improve the attack performance in image space, Generative Adversarial Networks (GANs) were introduced for synthesizing high-quality samples [3, 19, 44]. Further, due to the great success of StyleGAN2 [18] in generating high fidelity images, [37] built upon this generator for higher sample realism. Though effective, these methods heavily depend on the distribution shift between the auxiliary and private data. For example, by pretraining on auxiliary datasets in terms of blurred or partially blocked images, [44] improved the identification accuracy of reconstructed images. [34] introduced a robust and flexible attack, which only built the target upon the independent image priors. Existing MI attacks have overlooked the catastrophic forgetting issue. In addressing this problem, we find that reusing historical information can be advantageous in improving the capture of the target data distribution while preserving diversity.

Moreover, several papers considered the black-box setting without access to a model's gradients [1, 2, 39, 40]. In this paper, we take a new perspective to address the white-box MI attacks. We aim to capture more identity-representative information from historically synthesized images. We strive for dynamic memory learning via defined prototypes, which helps to prevent forgetting during training, resulting in high threats to target models.

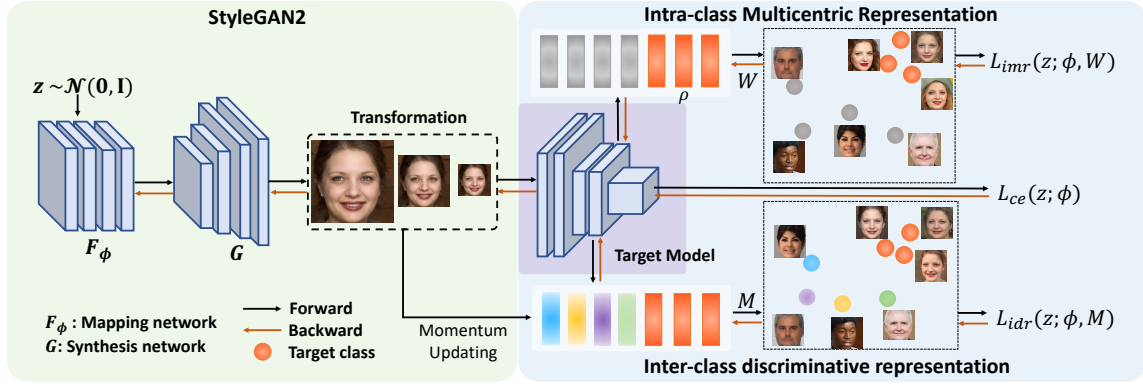


Figure 2: Overview of Dynamic Memory Model Inversion Attack. Given a target model, the sampled vector z from the Gaussian distribution is first transformed to a disentangled latent code with semantic meanings by Mapping Network. Then, the Synthesis network modifies this latent code to an image. With proposed IMR and IDR, the memory representations are modeled for updating Mapping Network and learnable W by back-propagating the proposed losses.

3 PROBLEM FORMULATION

In white-box MI attacks, attackers have full access to the target model trained on a private dataset $\mathcal{D} = \{(x_i, y_i), i \in (1, \dots, N)\}$, drawn from joint distribution $P_{\mathbb{X}, \mathbb{Y}}$, where $x_i \in \mathbb{X}$ and $y_i \in \mathbb{Y} = \{1, \dots, K\}$ denote the input image and the corresponding class label, respectively. For target K class classifier $f_c: \mathbb{X} \rightarrow \mathbb{Y} \in \mathbb{R}^K$, the goal of is to synthesis $\mathcal{D}^S\{\hat{x}_i|y_i = y_t\}$ to approximate the training data $\mathcal{D}^X\{x_i|y_i = y_t\}$, where y_t is the specific target label.

However, when x is high-dimensional data, directly optimizing the objective may directly result in meaningless features for generated results. To address this issue, generative models are introduced to generate high fidelity and semantic images [4, 37, 46]. Thus the attack process switches to producing private data that matches the target model using a generative model. As shown in Figure 2, we use a pre-trained StyleGAN [17] with auxiliary knowledge as the generative models, which the attack’s knowledge of the target model’s classification intent. Instead of feeding the input latent code z directly to the beginning of the network, the *mapping network* $F_\phi(z)$ first converts it to an intermediate latent code, which is then fed into a *synthesis network* G to synthesize images. Thus, the optimization of the x becomes the optimization of the network parameter ϕ in the mapping network, and the MI attack is defined as follows:

$$\min_{\phi} \mathcal{L}(f_c(\hat{x}), y_t), \hat{x} = G(F_\phi(z)), z \sim \mathcal{N}(0, I) \quad (1)$$

To avoid catastrophically forgetting previously learned knowledge, in the following section, we propose a solution for optimizing the above objective function by constructing progressive prototypes to reuse historical knowledge.

4 METHODOLOGY

We propose a Dynamic Memory Model Inversion Attack (DMMIA) to improve the generated results by exploring representation prototypes from two clues: 1) Intra-class Multicentric Representation (IMR). 2) Inter-class Discriminative Representation (IDR). The overview of our method is depicted in Figure 2.

4.1 Intra-class multicentric representation

To take full advantage of learned knowledge, we design an intra-class multicentric representation (IMR) prototype module. IMR represents the target class with multiple concepts through learnable prototypes, where each prototype represents a specific concept. we find that the generated samples tend to overfit by emphasizing the specific features for the target model, thereby losing the diversity within the class. For learning multiple concepts for each class by multicentric prototypes, we divide the learnable prototypes into positive and negative components. The positive part captures the salient characteristics associated with the target, while the negative part represents undesirable features to be avoided. By aligning the embedding feature of the generated sample with the prototypes, the IMR module effectively increases the sample diversity.

Formally, we define a set of trainable parameters $W \in \mathbb{R}^{N_w \times N_d}$ as learnable prototypes, where the positive prototype set $W^P = \{w_i \in \mathbb{R}^{1 \times N_d}, i \in [1 : \rho]\}$ records multiple concepts for the target class and negative prototype set $W^n = \{w_i \in \mathbb{R}^{1 \times N_d}, i \in [\rho + 1 : N_w]\}$ are prototypes used to distinguish from the target class. Let $f_e(\hat{x})$ denote a tensor image feature of dimension N_d , obtained by passing a generated image \hat{x} through the feature extractor of the target model. We interpret each positive prototype in W^P as a concept in the feature space of the target class. Then, the probability of a concept $f_e(\hat{x})$ in feature space belonging to the target class can be defined as:

$$p_{imr}(\hat{x}) = \frac{\sum_{i=1}^{\rho} \exp(f_e(\hat{x})^T w_i)}{\sum_{j=1}^{N_w} \exp(f_e(\hat{x})^T w_j)} \quad (2)$$

IMR aims to find the mapping network parameters ϕ and prototypes W that maximize the log-likelihood function of the generated samples. Finally, IMR learns target class concepts by minimizing:

$$\mathcal{L}_{imr}(z; \phi, W) = -\log p_{imr}(\hat{x}), \quad \text{where } \hat{x} = G(F_\phi(z)) \quad (3)$$

Consequently, through the learning of multiple concepts of the target class via prototype learning, IMR increases the sample diversity from the perspective of intra-class relations.

Algorithm 1 DMMIA

```

1: Input: Synthesis net  $G$ ; Mapping net  $F_\phi$ ; Target net  $f$ ; Momentum coefficient  $r$ ; Training epoch  $T$ 
2: Initialize: IMR set  $W$ ; Empty IDR set  $M$ 
3: procedure UPDATE( $W, M, F_\phi$ )
4:   while Training step  $i < T$  do
5:      $z_i \leftarrow \mathcal{N}(0, I)$  ▷ Sample latent vector
6:      $\hat{x}_i \leftarrow G(F_\phi(z_i))$ 
7:      $\phi_{i+1} \leftarrow \nabla_{\phi_i} \mathcal{L}_{\text{DMMIA}}(\hat{x}_i, y_t, \phi_i, W_i, M_i)$ 
8:      $W_{i+1} \leftarrow \nabla_{W_i} \mathcal{L}_{\text{imr}}(\hat{x}_i, y_t, W_i)$  ▷ Fix  $\phi_{i+1}$ 
9:      $M_{i+1} \leftarrow rM_i + (1-r)M'_i$  ▷ update memory bank
10:   end while
11: end procedure

```

4.2 Inter-class discriminative representation

Besides exploring the target representation from intra-relation via IMR, we design an inter-class discriminative representation (IDR) module. As aforementioned, the previously generated unique features are generally discarded during optimization. IDR defines a set of non-parameter prototypes by maintaining a memory bank, where the embedding features $f_e(\hat{x})$ of generated images are stored for prototype metric learning. Specifically, historical features of input images are injected into the IDR prototype set M_c according to their predicted class $c = \arg \max p(\hat{x})$, where $p(\hat{x})$ represents the prediction probability of target model. We denote the IDR prototypes as $M \in \mathbb{R}^{K \times N_d}$, where $M_i \in \mathbb{R}^{N_d}$ records the feature in memory for the i -th class. Then, IDR repels different categories by measuring the similarity between the current embedding feature $f_e(\hat{x})$ and each class of discriminative prototypes. The probability of a generated sample \hat{x} belonging to the target class is denoted as:

$$p_{\text{idr}}(\hat{x}) = \frac{\exp(f_e(\hat{x})^T M_{y_t})}{\sum_{i=1}^K \exp(f_e(\hat{x})^T M_i)} \quad (4)$$

Finally, $f_e(\hat{x})$ is aligned with corresponding prototypes in embedding space by:

$$\mathcal{L}_{\text{idr}}(z; \phi, M) = -\log p_{\text{idr}}(\hat{x}), \quad \text{where } \hat{x} = G(F_\phi(z)) \quad (5)$$

Momentum Updating. With the updating of F_ϕ of IDR during training, the memory bank is updated by the current image feature $f_e(\hat{x})$. To update the memorized prototypes in a more stable way, we propose to use a momentum update as follows:

$$M_c = rM_c + (1-r)M'_c \quad (6)$$

where $c = \arg \max p(\hat{x})$ is the predicted class and $r \in [0, 1]$ is a momentum coefficient. M'_c indicates the mean of current prototype features of the c -th class. With progressively-updated memorized prototypes, \mathcal{L}_{idr} represents the privacy data from historical knowledge. Consequently, IDR encourages the generated images in the same class to have more distinguishable characteristics, *i.e.*, revealing more privacy-sensitive information.

4.3 Overview of the training

Following a previous attack method [44], cross-entropy loss [7] \mathcal{L}_{ce} is used to enforce the inverted images to be correctly classified

as the target label y_t . With the memory learning loss defined, the objective loss function is:

$$\mathcal{L}_{\text{DMMIA}} = \mathcal{L}_{\text{ce}} + \lambda_1 \cdot \mathcal{L}_{\text{imr}} + \lambda_2 \cdot \mathcal{L}_{\text{idr}} \quad (7)$$

where λ_1 and λ_2 are scalars balancing the influence of two prototypes. We remark that the ϕ and W are optimized alternately, and the details of DMMIA are presented in Algorithm 1. Firstly, we sample a predetermined number of latent vectors z , and then only the 200 latent vectors with the highest prediction scores are used for optimization.

5 ANALYSIS ON THE DIVERSITY OF DMMIA

In this subsection, we analyze how DMMIA affects the intra-class diversity, which is an important metric of a good MI attack. We analyze the relationship between the probability distribution and the memory projected probability distribution from the perspective of KL-divergence. Without loss of generality, we assume $N_w = K$, the IMR and IDR become $W \in \mathbb{R}^{K \times N_d}$ and $M \in \mathbb{R}^{K \times N_d}$. We define $p(y|\hat{x}) = \text{softmax} f_c(\hat{x})$ as the probability distribution on target model under the \mathcal{L}_{ce} supervision. The memory projected probability distribution is then $q(y|\hat{x}) = \text{softmax} \left((W + M)^T f_e(\hat{x}) \right)$.

DEFINITION 1. Let $f: \mathbb{X} \rightarrow \mathbb{Y}$ be a smooth mapping. When $W \in \mathbb{R}^{K \times N_d}$ and $M \in \mathbb{R}^{K \times N_d}$, $(W + M)^T f_e(\hat{x})$ can be represented as a linear transformation of $f_e(\hat{x})$. There exists an η such that $f_e(\hat{x} + \eta) = (W + M)^T f_e(\hat{x})$.

DEFINITION 2. Let \mathbb{X} be a Riemannian manifold with the Fisher information matrix $G_{\hat{x}}$ as its metric tensor. $s = [p_1(\hat{x}), \dots, p_K(\hat{x})]^T$ is the output of the softmax layer in function f , where G_s is the Fisher information matrix associated with s .

According to the definition, $\hat{x} + \eta$ represents the generated optimal sample corresponding to \mathcal{L}_{imr} and \mathcal{L}_{idr} . We can use $p(y|\hat{x} + \eta)$ to approximate the distribution of $q(y|\hat{x})$. Thus, our goal is converted to observe the KL-divergence between $p(y|\hat{x})$ and $p(y|\hat{x} + \eta)$. During the optimization, \hat{x} and $\hat{x} + \eta$ are progressively aligned to the specified target class, enabling consistent decreasing KL-divergence between the corresponding probability distribution from target models. Assuming that a sufficiently small η is obtained by Algorithm 1, an intriguing property of DMMIA is defined as follows.

THEOREM 1. Let $\hat{x} = G(F_\phi(z))$ be the synthesised image. Minimizing the KL-divergence between the distribution $p(y|\hat{x})$ and $p(y|\hat{x} + \eta)$ is encouraged by optimizing the $\mathcal{L}_{\text{DMMIA}}$, which is equivalent to: $\arg \min \sum_{i=1}^K \frac{1}{p_i}$, s. t. $\sum_{i=1}^K p_i = 1$. Then, we have $p_1 = p_2 = \dots = p_K = \frac{1}{K}$, where p_i is the prediction probability of i -th class.

PROOF. Let y be the random variable ranging from y_1 to y_k . The KL-divergence between the distribution $p(y|\hat{x})$ and $p(y|\hat{x} + \eta)$ can be expanded via the second-order Taylor expansion:

$$D_{\text{KL}}(p(y|\hat{x}), p(y|\hat{x} + \eta)) = \mathbb{E}_y [\log \frac{p(y|\hat{x})}{p(y|\hat{x} + \eta)}] \approx \frac{1}{2} \eta^T G_{\hat{x}} \eta$$

$$G_{\hat{x}} = \mathbb{E}_{x \sim \mathbb{X}, y \sim p(y|\hat{x})} \left[g_x(\hat{x}, y) g_x(\hat{x}, y)^T \right] \quad (8)$$

where $G_{\hat{x}}$ is the fisher information matrix of \hat{x} , and $g_x(\hat{x}, y)$ is the gradient to input \hat{x} w.r.t on the loss for label y . It is difficult to compute the high dimension matrix $G_{\hat{x}}$. We follow [33]

to formulate $G_{\hat{x}}$ as a new matrix G_s through $G_{\hat{x}} = J^T G_s J$. G_s is the fisher information matrix of the output of the softmax layer $s = [p_1(\hat{x}), \dots, p_K(\hat{x})]^T$, which has been defined in Definition 2. The term J is the Jacobian matrix of f_c and can be computed by $J = \frac{\partial s_i}{\partial \hat{x}}$. To this end, G_s is a $K \times K$ positive definite matrix and formulated as:

$$G_s = \mathbb{E}_{s \sim \mathbb{Y}, y \sim p(y|s)} [g_s(s, y) g_s(s, y)^T] \quad (9)$$

where $g_s(s, y)$ is the gradient to s w.r.t on the loss for label y . Then, Equation 10 becomes:

$$\eta^T G_{\hat{x}} \eta = \eta^T J^T G_s J \eta \quad (10)$$

During the optimization of GANs, \hat{x} and $\hat{x} + \eta$ are aligned to the target class while gradually minimizing the KL-divergence between them. This minimization decreases the variances of η , while seeking the smallest eigenvalue of $G_{\hat{x}}$, *i.e.*, minimizing the eigenvalues of G_s . The trace of metric equals the summation of all eigenvalues, which are all positive. Hence, minimizing eigenvalues is equivalent to finding the smallest trace. The trace of G_s can be computed as:

$$\begin{aligned} \text{tr}(G_s) &= \text{tr}(\mathbb{E}_{s \sim \mathbb{Y}, y \sim p(y|s)} [g_s(s, y) g_s(s, y)^T]) \\ &= \text{tr}(\mathbb{E}_s [(\nabla_s \log p(y|s)) (\nabla_s \log p(y|s))^T]) \\ &= \int_{\mathbb{Y}} p(y|s) [\text{tr}(\nabla_s \log p(y|s))^T (\nabla_s \log p(y|s))] \quad (11) \\ &= \sum_{i=1}^K p_i \sum_{j=1}^K (\nabla_{p_j} \log p_i)^2 = \sum_{i=1}^K \frac{1}{p_i} \end{aligned}$$

Then, minimizing $\text{tr}(G_s)$ is equivalent to finding the optimal solution of $\arg \min \sum_{i=1}^K \frac{1}{p_i}$, s. t. $\sum_{i=1}^K p_i = 1$.

Different from general-purpose, which only matches the target class-specific feature, the memory-guided prototype learning enforces F_ϕ optimizing towards uniform distribution $\mathcal{U}(1, k)$. It may be different from intuition, but this intriguing property is no harm due to the main term \mathcal{L}_{ce} in the loss Equation 7. Together with the above analysis, we can obtain the following theorem.

THEOREM 2. *The geodesic distance in the probability space is always no larger than the corresponding distance in the data space:*

$$\mathcal{D}(\hat{x}_i, \hat{x}_j) \geq \mathcal{D}(\text{softmax}(f_c(\hat{x}_i)), \text{softmax}(f_c(\hat{x}_j))) \quad (12)$$

where \mathcal{D} is the geodesic distance.

PROOF. Note that for most neural networks, the dimensionality of s is much less than that of \hat{x} . That is to say, η is mapped by J from high dimensional data space to low dimensional probability space. Thus, f_c is a surjective mapping and $G_{\hat{x}}$ is a degenerative metric tensor. Following [45], the geodesic distance in the probability space is always no larger than the corresponding distance in the data space. Assuming that \hat{x}_i and \hat{x}_j are two generated images from the same target class y_t . Then, we have the inequality as Equation 12.

Without memory prototypes, the target model predicted probability is updated toward a pure point $p(y|\hat{x}) = [0, \dots, p_{y_t}, \dots, 0]$, among which the valid values are only those with an index y_t and all the others 0. However, Theorem 1 shows that the memory prototypes cause the F_ϕ to update toward a uniform distribution while conforming to private target data. Thus DMMIA further leads to a mixed probability distribution together $p(y|\hat{x})$ with $\mathcal{U}(1, K)$. This

objective probability distribution is more likely to attain high variance than pure $p(y|\hat{x})$. Thus, under the DMMIA scenario, the floor level of the geodesic distance between any two generated images in probability space is larger than that of baseline. At a higher level of data space, according to Theorem 2, the distance of generated two images is increased consistently. It indicates that these prototypes can increase the sample similarity. In a broader sense, the theorem confirms the validity of our approach.

6 EXPERIMENTS

6.1 Training Setups

Dataset. We evaluate DMMIA on two face image datasets, including CelebFaces Attributes [25] (CelebA) and FaceScrub Dataset [27]. CelebA contains 10,177 identities with coarse alignment. The train-test-splits setting is followed with [34]. FaceScrub is consisted of face images of male and female celebrities, with about 200 images per person. Moreover, we validate the effectiveness of DMMIA on Stanford Dogs dataset [8] and hand-written image dataset MNIST [23]. Due to cost concerns, we used 1/10 classes in ablation studies. More details about the dataset can be referred to Appendix B.

Models. We implement several popular target networks with different depths and architectures, including ResNet-18 [12] nets on CelebA and FaceScrub. In the extended evaluation section, we attack the ResNeSt-101 [43], ResNet-152 [12] and DenseNet-169 [15] networks separately on target datasets. For generators, we consider StyleGAN2 with Flickr-Faces-HQ (FFHQ) [17], MetFaces [16] and Animal Faces-HQ Dogs (AFHQ) prior for inversion. FFHQ offers higher quality human face images, while MetFaces is a face dataset extracted from the Metropolitan Museum of Art collection, which has a large distribution shift from real face images. Besides, AFHQ [6] is used as a prior for attacking Stanford Dogs models.

Metrics. We evaluate the MI attack performance from the perspective of target attack accuracy, sample diversity, and sample realism. Acc@1 and Acc@5 are defined as the top-1 and top-5 accuracy given a classifier for evaluation, respectively. We choose the Inception-v3 [35] trained on specific target datasets to test the accuracy over 50 generated samples for each target class. It is worth noting that this evaluation model is different from the target model. Higher accuracy indicates that the synthesized images reveal more private information about the target label. Furthermore, we measure the image quality by computing Frechet Inception Distance (FID) [13] between reconstructions and private target images. For a comprehensive comparison, we compute the shortest feature distance of each generated image to target training samples. l_{eval}^2 and l_{face}^{cos} represent the feature distance on the evaluation model Inception-v3 [35] and a pre-trained FaceNet [30], respectively. Moreover, we report Precision-Recall [22] and Coverage-Density [26] metrics to quantify the intra-class diversity of synthesized samples explicitly.

Attack implementation. The image prior assumption for pre-training StyleGAN2 models allows the target data and the auxiliary data are meant to be disjoint. The size of sampled latent vectors z is 5000 for CelebA models and 2000 for FaceScrub and Stanford Dogs models. To train the mapping network $F_\phi(z)$ in StyleGAN2 and IMR prototypes W , we use the Adam optimizer with the learning rate

DATASET	METHOD	\uparrow Acc@1	\uparrow Acc@5	\downarrow l^2_{eval}	\downarrow l^{cos}_{face}	\downarrow FID	\uparrow PRECISION	\uparrow RECALL	\uparrow DENSITY	\uparrow COVERAGE
CelebA	GMI [44]	9.76	15.22	225.41	1.7800	151.06	0.0829	0.0283	0.0366	0.0379
	KED [4]	14.71	28.69	197.03	1.4023	132.34	0.0097	0.0072	0.0056	0.0011
	VMI [37]	59.74	74.32	152.24	0.8871	79.31	0.0210	0.0198	0.0238	0.0320
	MIRROR [2]	77.90	83.40	138.62	0.9991	78.12	0.1523	0.0246	0.6080	0.2873
	PPA [34]	87.76	96.50	129.02	0.7218	59.73	0.2856	0.0513	0.7304	0.4123
	DMMIA	94.02	99.33	123.54	0.7167	58.29	0.2956	0.0581	0.7383	0.4270
FaceScrub	GMI [44]	12.30	21.96	163.43	1.4880	199.61	0.0082	0.0176	0.0174	0.0094
	KED [4]	16.05	24.74	152.40	1.2075	157.63	0.0194	0.0018	0.0058	0.0029
	VMI [37]	51.77	78.94	142.78	0.9071	98.09	0.0343	0.0307	0.0329	0.0455
	MIRROR [2]	82.31	91.74	139.68	0.9511	63.82	0.0210	0.0238	0.0605	0.0378
	PPA [34]	85.76	97.56	114.99	0.7155	49.93	0.1427	0.0462	0.1777	0.1870
	DMMIA	93.54	99.28	110.73	0.6392	47.48	0.1513	0.0571	0.1894	0.1906

Table 1: Comparison with state-of-the-art methods against ResNet-18 trained on CelebA and FaceScrub respectively. \uparrow and \downarrow symbolize that higher and lower scores give better attack performance.

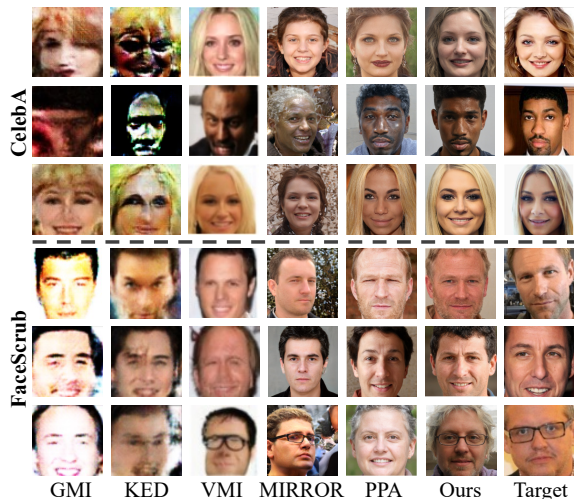


Figure 3: Visual comparison of attack results against the ResNet-18 trained on CelebA and FaceScrub.

0.005 and batch size of 16, $\beta_1 = 0.1$ and $\beta_2 = 0.1$ [20]. The training epochs on FaceScrub, Stanford Dogs, and CelebA experiments are set as 50, 50, and 70, respectively. Besides, the transformation operation follows [34]. We set the prototype number $N_w = 500$ with $\rho = 250$, $\lambda_1 = 0.3$ and $\lambda_2 = 0.7$. r is set as 0.7. We perform all our experiments on 8 NVIDIA RTX 3090 GPUs, which are based on CUDA 11.4 and Python 3.8.10. For more details of the implementations, please refer to Appendix B.

6.2 Experiment results

To thoroughly evaluate our DMMIA, we conduct experiments on two privacy-preserving human-face datasets and two non-privacy datasets, accompanied by a detailed ablation study. Additionally, we have analyzed the computational complexity of DMMIA, and find that it adds only a little extra computational cost during training compared to the baseline, with no extra cost in inference attacks.

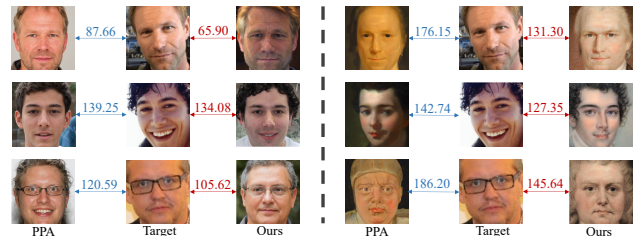


Figure 4: Visual results against the ResNeSt-101 with FFHQ (left) and MetFaces (right) prior. We show the quantitative similarity between the generated images and targets using $\downarrow l^2_{eval}$ metric. The images produced via DMMIA have lower distance values, particularly when the prior distribution differed significantly from the target image distribution.

Benchmark results on privacy data. We conduct a comprehensive evaluation of the proposed DMMIA compared with several MI attacks, as shown in Table 1. The generators for all methods are pre-trained on the FFHQ dataset and try to reveal the private data in CelebA and FaceScrub datasets. We find that DMMIA can achieve state-of-the-art attack accuracy. For CelebA datasets, the Acc@1 of DMMIA is higher than PPA by 6.26%, while having a smaller distance between generated images and private data. The improved four diversity metrics indicate that our method can learn more characteristics of facial images per class. Additionally, DMMIA outperforms all MI attacks on recovering the FaceScrub dataset, achieving the highest attack accuracy 93.54% with better sample realism and diversity. We provide generated samples in Figure 3. Notice that the synthesized images by GMI and KED are at low resolution 64×64 pixels. Besides, GMI and KED can not create realistic samples in our setting. VMI is not effective in generating face images with high fidelity. The faces inverted by MIRROR and PPA are more human-recognizable than the attacks mentioned above. However, the images generated using DMMIA show maximum similarity with the target privacy data.

	PRIOR	METHOD	\uparrow Acc@1	\downarrow l^2_{eval}	\downarrow l^{\cos}_{face}	\downarrow FID	\uparrow DIV
CelebA	FFHQ	PPA	91.68	135.51	0.7303	58.16	0.3684
		DMMIA	94.06	132.45	0.7030	55.92	0.3723
	Met.F	PPA	50.52	158.30	1.0708	89.74	0.1837
		DMMIA	70.58	149.37	0.9821	89.33	0.1895
FaceScrub	FFHQ	PPA	75.80	120.70	0.7901	69.41	0.1419
		DMMIA	86.98	120.00	0.7526	68.93	0.1466
	Met.F	PPA	46.20	137.86	0.9524	94.78	0.1276
		DMMIA	68.70	131.92	0.8511	94.32	0.1579

Table 2: Comparison results with various target datasets and image priors against ResNet-152 trained on CelebA and FaceScrub datasets. Met.F stands for MetFaces dataset.

ARCHITECTURE	METHOD	\uparrow Acc@1	\downarrow l^2_{eval}	\downarrow FID	\uparrow Div
ResNeSt-101	PPA	97.60	42.57	64.00	0.3050
	DMMIA	99.25	41.87	63.43	0.3122
ResNet-152	PPA	89.00	40.75	63.32	0.2429
	DMMIA	97.50	39.71	61.46	0.2458
DenseNet-169	PPA	95.00	38.45	63.17	0.2893
	DMMIA	96.80	37.16	61.73	0.3082

Table 3: Comparison of attack results on Stanford Dogs dataset with FFHQ image prior. The DIV is the mean of PRECISION, RECALL, DENSITY and COVERAGE, capturing the intra-class diversity of the generated samples.

Extended evaluation. We compare DMMIA with the PPA with FFHQ and MetFaces image priors, as shown in Table 2. See Appendix C for more experiments on attacking ResNeSt-101 and DenseNet-169. We find that DMMIA achieves higher attack accuracy across multiple target models. For example, when attacking ResNet-152 trained on CelebA with FFHQ prior, the Acc@1 of DMMIA is higher than PPA by 2.38%. Meanwhile, the sample realism and diversity of DMMIA outperform PPA in all cases. With the loosened image prior, DMMIA yields significantly better attack performance than baseline. For attacking FaceScrub with Metfaces prior, the Acc@1 of DMMIA outperforms PPA by a large margin of 22.5%. The distance between generated and target images on the evaluation model decreases by 5.94 on l^2_{eval} . Figure 4 and the qualitative evaluation both support our findings, showing that the generated samples by DMMIA had lower $\downarrow l^2_{eval}$ than the target data, particularly when attacking without knowledge of sensitive attributes using StyleGAN2 trained on MetFaces. These results suggest that the dynamic memory prototype enhances both image inversion and diversity in various settings. However, the study also revealed a significant drop in DMMIA’s Acc@1 from 94.06% to 70.58% when transitioning from FFHQ to MetFaces prior, indicating that the success of the attacks heavily depended on the diversity of prior information.

Benchmark results on non-privacy data. We also provide the results on attacking the Stanford Dogs and MNIST dataset.

Results on Stanford Dogs. The results in Table 3 show that DMMIA surpasses PPA on three target models regarding attack success accuracy. As confirmed by the FIDs, the average quality of our DMMIA is higher than PPA. We visualize the generated images in Figure 5a. It indicates the consistent performance of DMMIA across different types of images. Consequently, by representing target data

METHOD	GMI [44]	KED [4]	VMI [37]	PPA [34]	DMMIA
\uparrow Acc@1	27.53	38.61	28.60	45.60	48.72
\downarrow FID	90.64	72.41	84.23	58.05	57.43

Table 4: Comparison results on attacking ResNet-18 with MNIST.

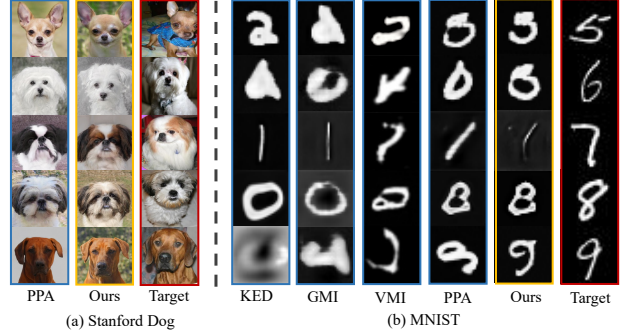


Figure 5: (a) Visual results against the ResNeSt-101 trained on Stanford Dog dataset. (b) Visual results against the ResNet-10 trained on MNIST dataset.

from historical information, DMMIA can capture more target-class sensitive information and expand the sample diversity.

Results on MNIST. To further show the effectiveness of DMMIA and demonstrate its significance, we have run more experiments on MNIST [23]. To ensure the StyleGAN2 contains hand-written image priors, we use all of the images with labels 5, 6, 7, 8, 9 as a public set while attacking the images with labels 0, 1, 2, 3, 4. All the images are resized to 32×32 . The details of this experimental setting refer to the Appendix B. In Table 5, the “Acc@1” column shows that the attack success rate promotion of DMMIA on MNIST is 3.12 compared to state-of-the-art methods. Thus, DMMIA is a more general method that works better for both natural and facial images and can be more practical.

We compare the reconstruction quality of different attacks in Figure 5b. The images produced by DMMIA can capture most of the target class characteristics. It can also be found that the generated images with successful attacks depend much on the image prior (*i.e.*, images with labels [0,1,2,3,4]). The attack results on MNIST further demonstrate the superiority of DMMIA.

6.3 Ablation study

We conduct a series of experiments to examine the impact of several key aspects on the performance of the proposed DMMIA attack. Specifically, we analyze the influence of different values of λ_1 and λ_2 (representing the impact of IMR and IDR on the model inversion attack), the prototype size N_w , the prototype size ρ , and the momentum coefficient r . Our evaluation was conducted using ResNet-18 trained on CelebA as the target model and StyleGAN2 with FFHQ as the image prior for the attack.

Effect of λ_1 and λ_2 . λ_1 and λ_2 are the hyper-parameters to balance \mathcal{L}_{ce} and \mathcal{L}_{imr} with \mathcal{L}_{idr} . Specifically, setting $\lambda_1 = 0$ or $\lambda_2 = 0$ allows us to evaluate the individual effect of prototype IDR and IMR. As shown in Figure 6, to better validate the two components of DMMIA, studies are performed in a grid-search way. In panels

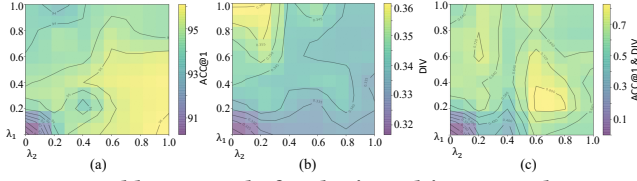


Figure 6: Ablation study for the λ_1 and λ_2 on attack success rate and sample diversity, echoing (a): Acc@1 and (b): DIV. Chosen optimal hyper-parameters including both Acc@1 and DIV, echoing (c).

(a) and (b), we report the attack success rate and sample diversity over various λ_1 and λ_2 . The optimal λ_1 and λ_2 are determined by $[Normalize(Acc@1) + Normalize(DIV)]/2$, shown in panel (c).

Notably, both IMR and IDR can benefit the attack performance. Larger λ_2 , *i.e.*, DMMIA with the higher weight of IDR can achieve better performance on attack accuracy, as shown in Figure 6a. It indicates that the inter-class representation of IDR helps to capture more sensitive information of the targets. Shown in Figure 6b, the diversity performance of DMMIA is mainly led by λ_1 , *i.e.*, the weight of IMR. It verifies the advantages of IMR that representing the target class distribution can encourage the F_ϕ to be more exploratory and augment sample diversity. Finally, DMMIA simultaneously considers the intra-relation and inter-relation of the privacy dataset, resulting in the best trade-off ($\lambda_1 = 0.3$ and $\lambda_2 = 0.7$) between sample quality and sample diversity. More results on the effect of IMR and IDR refer to the Appendix C.

N_w	\uparrow Acc@1	\downarrow l^2_{eval}	\downarrow l^{cos}_{face}	\downarrow FID	\uparrow Div
100	95.25	131.42	0.7449	90.17	0.3097
500	95.00	131.28	0.7448	89.03	0.3532
900	94.75	131.64	0.7471	89.97	0.3580

Table 5: Results of DMMIA, with different prototype size N_w , against ResNet-18 trained on CelebA.

Effect of prototype size N_w . The proposed intra-class multi-centric representation introduces a learnable prototype set $W \in \mathbb{R}^{N_w \times N_d}$. We present the results of the study conducted to investigate the impact of prototype size N_w . ρ is set to be half of N_w . Echoing Table 5, DMMIA with IMR can achieve more than 20% DIV improvement as the prototype size increases from 100 to 900. This suggests that IMR can effectively capture visual concepts of the target class through multi-centric representation. However, to balance performance with computation, we set the prototype size N_w to 500 for the final experiments.

ρ	\uparrow Acc@1	\downarrow l^2_{eval}	\downarrow l^{cos}_{face}	\downarrow FID	\uparrow Div
100	95.00	131.16	0.7484	89.73	0.3361
250	95.00	131.28	0.7448	89.03	0.3532
400	94.25	132.76	0.7563	89.16	0.3710

Table 6: Ablation study of ρ in IMR, which is the number of positive prototypes in W .

Effect of prototype size ρ . To evaluate the effect of prototype size of IMR on the attack performance, we vary the number of positive prototypes, represented by ρ , as shown in Table 6. As ρ

rises from 100 to 400, *i.e.*, more concepts for the target class are represented, which leads to an improvement in the diversity of the generated images. However, a larger value of ρ may result in a trade-off between attack accuracy and sample diversity. To balance these two factors, we set $\rho = 250$ as the optimal value for achieving better results.

r	\uparrow Acc@1	\downarrow l^2_{eval}	\downarrow l^{cos}_{face}	\downarrow FID	\uparrow Div
0.1	94.75	132.25	0.7482	89.08	0.3332
0.3	95.00	131.96	0.7488	89.87	0.3477
0.5	95.00	132.53	0.7516	89.58	0.3662
0.7	95.75	131.48	0.7446	88.44	0.3413
0.9	95.25	132.52	0.7482	88.35	0.3591

Table 7: Ablation study of r . The performance is evaluated on attacking ResNet-18 with CelebA.

Effect of r . The momentum coefficient r controls the updating the smoothness of the memory bank in IDR. As shown in Table 7, our method is generally not sensitive to the selection of r . We set $r = 0.7$ for the optimal results. Noted that using too fast updating (*e.g.*, 0.1) causes a small performance drop in attack accuracy. This is mainly because the updating of the memory bank is jointly conducted with the model training. If the memory bank is updated too quickly, it may not have enough time to properly learn from the prototypes being stored in the memory bank, which hinders the capacity of inter-class discriminability.

6.4 Complexity Analysis

Noted that incorporating DMMIA into the training process incurs minimal additional computational cost compared to the baseline method, with no extra cost incurred during inference attacks. Specifically, the time complexity of IMR and IDR during training is $O((K + N_w)N_dN_d)$. In terms of the attack on ResNet-18, it adds approximately 0.73M flops, which is negligible compared to the overall model. Additionally, our method does not add any extra parameters to the generative model, *i.e.*, it incurs no additional computational cost during the generation process.

7 CONCLUSION AND FUTURE WORK

In this paper, we propose a Dynamic Memory Model Inversion Attack (DMMIA), which improves the model inversion by reusing the memorized knowledge. Specifically, DMMIA constructs an intra-class multicentric representation (IMR) term and an inter-class discriminative representation (IDR) term. The learnable IMR models multiple concepts for representing the target class, which benefits from increasing sample diversity. Meanwhile, IDR injects the memorized knowledge into non-parametric prototypes to enforce the representations away from different categories, thus enhancing target class discriminability. Overall, DMMIA reports the state-of-the-art attack performance on multiple benchmarks. We will explore how to apply DMMIA on black-box model inversion attacks in the future, where the attacker cannot obtain the information of the model and can only get the prediction result by querying the target model.

REFERENCES

- [1] Ulrich Aivodji, Sébastien Gambs, and Timon Ther. 2019. Gamin: An adversarial approach to black-box model inversion. *arXiv preprint arXiv:1909.11835* (2019).
- [2] Shengwei An, Guanhong Tao, Qiuling Xu, Yingqi Liu, Guangyu Shen, Yuan Yao, Jingwei Xu, and Xiangyu Zhang. 2022. MIRROR: Model Inversion for Deep Learning Network with High Fidelity. In *Proceedings of the Network and Distributed Systems Security Symposium (NDSS 2022)*.
- [3] Si Chen, Ruoxi Jia, and Guo-Jun Qi. 2020. Improved techniques for model inversion attacks. (2020).
- [4] Si Chen, Mostafa Kahla, Ruoxi Jia, and Guo-Jun Qi. 2021. Knowledge-Enriched Distributional Model Inversion Attacks. In *Proceedings of the IEEE/CVF International Conference on Computer Vision*. 16178–16187.
- [5] WU Chenshen, L HERRANZ, LIU Xialei, et al. 2018. Memory replay GANs: Learning to generate images from new categories without forgetting [C]. In *The 32nd International Conference on Neural Information Processing Systems, Montréal, Canada*. 5966–5976.
- [6] Yunjeong Choi, Youngjung Uh, Jaehun Yoo, and Jung-Woo Ha. 2020. Stargan v2: Diverse image synthesis for multiple domains. In *Proceedings of the IEEE/CVF conference on computer vision and pattern recognition*. 8188–8197.
- [7] Pieter-Tjerk De Boer, Dirk P Kroese, Shie Mannor, and Reuven Y Rubinfeld. 2005. A tutorial on the cross-entropy method. *Annals of operations research* 134, 1 (2005), 19–67.
- [8] Jia Deng, Wei Dong, Richard Socher, Li-Jia Li, Kai Li, and Li Fei-Fei. 2009. Imagenet: A large-scale hierarchical image database. In *2009 IEEE conference on computer vision and pattern recognition*. Ieee, 248–255.
- [9] Matt Fredrikson, Somesh Jha, and Thomas Ristenpart. 2015. Model inversion attacks that exploit confidence information and basic countermeasures. In *Proceedings of the 22nd ACM SIGSAC conference on computer and communications security*. 1322–1333.
- [10] Matthew Fredrikson, Eric Lantz, Somesh Jha, Simon Lin, David Page, and Thomas Ristenpart. 2014. Privacy in pharmacogenetics: An {End-to-End} case study of personalized warfarin dosing. In *23rd USENIX Security Symposium (USENIX Security 14)*. 17–32.
- [11] Hongtao Guan, Yijie Wang, Xingkong Ma, and Yongmou Li. 2019. DCIGAN: a distributed class-incremental learning method based on generative adversarial networks. In *2019 IEEE Intl Conf on Parallel & Distributed Processing with Applications, Big Data & Cloud Computing, Sustainable Computing & Communications, Social Computing & Networking (ISPA/BDCloud/SocialCom/SustainCom)*. IEEE, 768–775.
- [12] Kaiming He, Xiangyu Zhang, Shaoqing Ren, and Jian Sun. 2016. Deep residual learning for image recognition. In *Proceedings of the IEEE conference on computer vision and pattern recognition*. 770–778.
- [13] Martin Heusel, Hubert Ramsauer, Thomas Unterthiner, Bernhard Nessler, and Sepp Hochreiter. 2017. Gans trained by a two time-scale update rule converge to a local nash equilibrium. *Advances in neural information processing systems* 30 (2017).
- [14] Seira Hidano, Takao Murakami, Shuichi Katsumata, Shinsaku Kiyomoto, and Goichiro Hanaoka. 2017. Model inversion attacks for prediction systems: Without knowledge of non-sensitive attributes. In *2017 15th Annual Conference on Privacy, Security and Trust (PST)*. IEEE, 115–11509.
- [15] Gao Huang, Zhuang Liu, Laurens Van Der Maaten, and Kilian Q Weinberger. 2017. Densely connected convolutional networks. In *Proceedings of the IEEE conference on computer vision and pattern recognition*. 4700–4708.
- [16] Tero Karras, Miika Aittala, Janne Hellsten, Samuli Laine, Jaakko Lehtinen, and Timo Aila. 2020. Training generative adversarial networks with limited data. *Advances in Neural Information Processing Systems* 33 (2020), 12104–12114.
- [17] Tero Karras, Samuli Laine, and Timo Aila. 2019. A style-based generator architecture for generative adversarial networks. In *Proceedings of the IEEE/CVF conference on computer vision and pattern recognition*. 4401–4410.
- [18] Tero Karras, Samuli Laine, Miika Aittala, Janne Hellsten, Jaakko Lehtinen, and Timo Aila. 2020. Analyzing and improving the image quality of stylegan. In *Proceedings of the IEEE/CVF conference on computer vision and pattern recognition*. 8110–8119.
- [19] Mahdi Khosravy, Kazuaki Nakamura, Yuki Hirose, Naoko Nitta, and Noboru Babaguchi. 2022. Model Inversion Attack by Integration of Deep Generative Models: Privacy-Sensitive Face Generation from a Face Recognition System. *IEEE Transactions on Information Forensics and Security* 17 (2022), 357–372.
- [20] Diederik P Kingma and Jimmy Ba. 2015. Adam: A Method for Stochastic Optimization. In *ICLR (Poster)*.
- [21] James Kirkpatrick, Razvan Pascanu, Neil Rabinowitz, Joel Veness, Guillaume Desjardins, Andrei A Rusu, Kieran Milan, John Quan, Tiago Ramalho, Agnieszka Grabska-Barwinska, et al. 2017. Overcoming catastrophic forgetting in neural networks. *Proceedings of the national academy of sciences* 114, 13 (2017), 3521–3526.
- [22] Tuomas Kynkäänniemi, Tero Karras, Samuli Laine, Jaakko Lehtinen, and Timo Aila. 2019. Improved precision and recall metric for assessing generative models. *Advances in Neural Information Processing Systems* 32 (2019).
- [23] Yann LeCun, Corinna Cortes, and Chris Burges. 2010. MNIST handwritten digit database.
- [24] Timothée Lesort, Hugo Caselles-Dupré, Michael Garcia-Ortiz, Andrei Stoian, and David Filliat. 2019. Generative models from the perspective of continual learning. In *2019 International Joint Conference on Neural Networks (IJCNN)*. IEEE, 1–8.
- [25] Ziwei Liu, Ping Luo, Xiaogang Wang, and Xiaoou Tang. 2015. Deep learning face attributes in the wild. In *Proceedings of the IEEE international conference on computer vision*. 3730–3738.
- [26] Muhammad Ferjad Naem, Seong Joon Oh, Youngjung Uh, Yunjeong Choi, and Jaehun Yoo. 2020. Reliable fidelity and diversity metrics for generative models. In *International Conference on Machine Learning*. PMLR, 7176–7185.
- [27] Hong-Wei Ng and Stefan Winkler. 2014. A data-driven approach to cleaning large face datasets. In *2014 IEEE international conference on image processing (ICIP)*. IEEE, 343–347.
- [28] Omkar M Parkhi, Andrea Vedaldi, and Andrew Zisserman. 2015. Deep face recognition. (2015).
- [29] Alec Radford, Jong Wook Kim, Chris Hallacy, Aditya Ramesh, Gabriel Goh, Sandhini Agarwal, Girish Sastry, Amanda Askell, Pamela Mishkin, Jack Clark, et al. 2021. Learning transferable visual models from natural language supervision. In *International conference on machine learning*. PMLR, 8748–8763.
- [30] Florian Schroff, Dmitry Kalenichenko, and James Philbin. 2015. Facenet: A unified embedding for face recognition and clustering. In *Proceedings of the IEEE conference on computer vision and pattern recognition*. 815–823.
- [31] Academy Medical Sciences. 2015. Stratified, personalised or P4 medicine: a new direction for placing the patient at the centre of healthcare and health education. (2015).
- [32] Ari Seff, Alex Beatson, Daniel Suo, and Han Liu. 2017. Continual learning in generative adversarial nets. *arXiv preprint arXiv:1705.08395* (2017).
- [33] Chaomin Shen, Yaxin Peng, Guixu Zhang, and Jinsong Fan. 2019. Defending against adversarial attacks by suppressing the largest eigenvalue of fisher information matrix. *arXiv preprint arXiv:1909.06137* (2019).
- [34] Lukas Struppek, Dominik Hintersdorf, Antonio De Almeida Correia, Antonia Adler, and Kristian Kersting. 2022. Plug & Play Attacks: Towards Robust and Flexible Model Inversion Attacks. *arXiv preprint arXiv:2201.12179* (2022).
- [35] Christian Szegedy, Vincent Vanhoucke, Sergey Ioffe, Jon Shlens, and Zbigniew Wojna. 2016. Rethinking the inception architecture for computer vision. In *Proceedings of the IEEE conference on computer vision and pattern recognition*. 2818–2826.
- [36] Hoang Thanh-Tung and Truyen Tran. 2018. On catastrophic forgetting in generative adversarial networks. *arXiv preprint arXiv:1807.04015* (2018).
- [37] Kuan-Chieh Wang, Yan Fu, Ke Li, Ashish Khisti, Richard Zemel, and Alireza Makhzani. 2021. Variational Model Inversion Attacks. *Advances in Neural Information Processing Systems* 34 (2021).
- [38] Chen Wu and Ming Yan. 2017. Session-aware information embedding for e-commerce product recommendation. In *Proceedings of the 2017 ACM on conference on information and knowledge management*. 2379–2382.
- [39] Xi Wu, Matthew Fredrikson, Somesh Jha, and Jeffrey F Naughton. 2016. A methodology for formalizing model-inversion attacks. In *2016 IEEE 29th Computer Security Foundations Symposium (CSF)*. IEEE, 355–370.
- [40] Ziqi Yang, Ee-Chien Chang, and Zhenkai Liang. 2019. Adversarial neural network inversion via auxiliary knowledge alignment. *arXiv preprint arXiv:1902.08552* (2019).
- [41] Mengyao Zhai, Lei Chen, Jiawei He, Megha Nawhal, Frederick Tung, and Greg Mori. 2020. Piggyback gan: Efficient lifelong learning for image conditioned generation. In *Computer Vision—ECCV 2020: 16th European Conference, Glasgow, UK, August 23–28, 2020, Proceedings, Part XXI 16*. Springer, 397–413.
- [42] Mengyao Zhai, Lei Chen, Frederick Tung, Jiawei He, Megha Nawhal, and Greg Mori. 2019. Lifelong gan: Continual learning for conditional image generation. In *Proceedings of the IEEE/CVF international conference on computer vision*. 2759–2768.
- [43] Hang Zhang, Chongruo Wu, Zhongyue Zhang, Yi Zhu, Haibin Lin, Zhi Zhang, Yue Sun, Tong He, Jonas Mueller, R Manmatha, et al. 2020. Resnest: Split-attention networks. *arXiv preprint arXiv:2004.08955* (2020).
- [44] Yuheng Zhang, Ruoxi Jia, Hengzhi Pei, Wenxiao Wang, Bo Li, and Dawn Song. 2020. The secret revealer: Generative model-inversion attacks against deep neural networks. In *Proceedings of the IEEE/CVF Conference on Computer Vision and Pattern Recognition*. 253–261.
- [45] Chenxiao Zhao, P Thomas Fletcher, Mixue Yu, Yaxin Peng, Guixu Zhang, and Chaomin Shen. 2019. The adversarial attack and detection under the fisher information metric. In *Proceedings of the AAAI Conference on Artificial Intelligence*, Vol. 33. 5869–5876.
- [46] Xuejun Zhao, Wencan Zhang, Xiaokui Xiao, and Brian Lim. 2021. Exploiting explanations for model inversion attacks. In *Proceedings of the IEEE/CVF International Conference on Computer Vision*. 682–692.